Journal of Power Sources 389 (2018) 169–177

Contents lists available at ScienceDirect

Journal of Power Sources

journal homepage: www.elsevier.com/locate/jpowsour

Enhanced performance of lithium-sulfur batteries with an ultrathin and lightweight MoS_2/carbon nanotube interlayer

Lingjia Yan[a,b], Nannan Luo[a], Weibang Kong[a,b], Shu Luo[a,b], Hengcai Wu[a,b], Kaili Jiang[a,b,c], Qunqing Li[a,b,c], Shoushan Fan[a,b], Wenhui Duan[a,c,**], Jiaping Wang[a,b,c,*]

[a] Department of Physics, Tsinghua University, Beijing 100084, China
[b] Tsinghua-Foxconn Nanotechnology Research Center, Tsinghua University, Beijing 100084, China
[c] Collaborative Innovation Center of Quantum Matter, Beijing 100084, China

HIGHLIGHTS

- MoS_2/CNT interlayer serves as both physical and chemical barrier for polysulfides.
- CNT film provides the electrodes with excellent conductivity.
- MoS_2 nanosheets form effective chemical interactions with the polysulfides.
- Li-S battery with the MoS_2/CNT interlayer displays enhanced cycling and rate performances.

ARTICLE INFO

Keywords:
Molybdenum sulfide/carbon nanotube
Interlayer
Polysulfides trapping
Lithium sulfur batteries

ABSTRACT

Ultrathin and lightweight MoS_2/carbon nanotube (CNT) interlayers are developed to effectively trap polysulfides in high-performance lithium–sulfur (Li–S) batteries. The MoS_2/CNT interlayer is constructed by loading MoS_2 nanosheets onto a cross-stacked CNT film. The CNT film with excellent conductivity and superior mechanical properties provides the Li–S batteries with a uniform conductive network, a supporting skeleton for the MoS_2 nanosheets, as well as a physical barrier for the polysulfides. Moreover, chemical interactions and bonding between the MoS_2 nanosheets and the polysulfides are evident. The electrode with the MoS_2/CNT interlayer delivers an attractive specific capacity of 784 mA h g^{-1} at a high capacity rate of 10 C. In addition, the electrode demonstrates a high initial capacity of 1237 mA h g^{-1} and a capacity fade as low as −0.061% per cycle over 500 charge/discharge cycles at 0.2 C. The problem of self-discharge can also be suppressed with the introduction of the MoS_2/CNT interlayer. The simple fabrication procedure, which is suitable for commercialization, and the outstanding electrochemical performance of the cells with the MoS_2/CNT interlayer demonstrate a great potential for the development of high-performance Li–S batteries.

1. Introduction

Nowadays, lithium-ion (Li-ion) batteries are widely used in portable electronic devices, electrical vehicles, and power grids. As these applications have developed over time, the energy requirements have increased. Batteries with high energy, power density, and specific capacity are in great demand [1]. Li–S batteries, with a theoretical capacity of 1672 mA h g^{-1} and specific energy density of 2600 W h kg^{-1}, have received extensive attention from many researchers. Sulfur cathodes display numerous advantages, such as high abundance of the raw material, relatively low cost, and environmental benignity. However, the application of Li–S batteries is hindered by the following challenges. First, both the active material (sulfur) and the discharge products (Li_2S_2/Li_2S) are electrically insulating. Second, the volume expansion during cycling reaches up to 80%. Last, and most important, the intermediate polysulfides (Li_2S_n, $4 \leq n \leq 8$) are highly dissolvable in the electrolyte and the shuttling of them between the electrodes results in a fast loss of capacity, i.e., the shuttle effect [2,3]. All these issues lead to a low utilization of sulfur, fast capacity fading, poor rate capability, and significant self-discharge behavior [4–6]. To overcome these difficulties, various approaches have been proposed for the design of sulfur composite cathodes. For example, various carbon matrices such as

* Corresponding author. Department of Physics and Tsinghua-Foxconn Nanotechnology Research Center, Tsinghua University, Beijing 100084, China.
** Corresponding author. Department of Physics, Tsinghua University, Beijing 100084, China.
E-mail addresses: dwh@phys.tsinghua.edu.cn (W. Duan), jpwang@tsinghua.edu.cn (J. Wang).

https://doi.org/10.1016/j.jpowsour.2018.04.015
Received 28 December 2017; Received in revised form 29 March 2018; Accepted 5 April 2018
Available online 11 April 2018
0378-7753/

carbon nanotubes [7–9], carbon nanofibers [10,11], graphene [12], and porous carbon [13,14] have been designed to provide cathodes with high electrical conductivity and a porous structure to enhance the electrical conductivity of the cathodes and suppress the shuttle effect. Conductive polymers [15–17] and metal oxides [18,19] have also been used to make composite sulfur cathodes. All these modifications can promote the electrochemical properties, accommodate the volume expansion, and restrain the diffusion of polysulfides to some extent. Nonetheless, the rapid capacity fading and severe self-discharge induced by the shuttle effect have not been fully addressed.

Separators, as an essential part of batteries, play an important role in blocking polysulfides at the cathode side and preventing them from shuttling to the anode to react with the lithium metal. Various separators and functional interlayers have been developed to suppress the diffusion of the polysulfides in Li–S batteries. For example, Manthiram's group revealed that a porous carbon interlayer between the sulfur cathode and the separator could effectively inhibit the shuttle effect of polysulfides, resulting in improved cycling performances of the electrode [20]. Kim and his co-workers reported that the dissolved polysulfides could be captured by introducing an acetylene black mesh; the electrodes demonstrated an enhanced rate and cycling results [21]. In fact, all these improvements can mainly be attributed to the excellent conductivity of the interlayer. The physical confinement of the polysulfides was not significant owing to the weak interaction between the highly polar polysulfides and the nonpolar carbon interlayer. Therefore, chemical interactions between the polysulfides and the separator or interlayer were necessary. Considering this, researchers have been investigating materials that can establish chemical bonding with polysulfides. For example, Nazar's group reported that ultrathin MnO_2 nanosheets formed surface-bound intermediates after reacting with polysulfides [22]. TiO_2 was applied as a highly effective polysulfide absorbent to improve the cycling performance by forming a Ti–S bond to suppress the dissolution of polysulfide [23]. Moreover, metal oxides/carbon and hydroxides/carbon interlayers such as ZnO nanowires/carbon nanofiber mat, magnesium borate hydroxide (MBOH)/CNT membrane, and NiFe layered double hydroxide (LDH) nanoplates/graphene layer, were designed to take advantages of both carbon matrix and metal oxides/hydroxides in improving the performance of Li-S batteries [24–26]. Compared with metal oxides, metal sulfides with metal–S bonds can bind polysulfides through the stronger S–S interaction and dipolar interaction of metal–sulfur bonds on the polarized surface. It has been reported in the literature that MoS_2 could effectively trap the polysulfides owing to the strong chemical interaction between MoS_2 and polysulfides [27–29]. However, it is still challenging to introduce MoS_2 into the Li–S system to effectively suppress the shuttle effect and improve the cell performance.

Herein, we report a simple and feasible strategy to develop MoS_2/CNT interlayers by uniformly loading MoS_2 nanosheets on a cross-stacked CNT film and taking advantage of the properties of both MoS_2 and CNTs. The MoS_2/CNT interlayer was ultrathin (2 μm) and lightweight (0.25 mg cm^{-2}). The CNT film provided excellent electrical conductivity for the sulfur electrode and a support skeleton for the dispersion of MoS_2, as well as a physical barrier for the diffusion of the polysulfide. The MoS_2 nanosheets further suppressed the shuttling effect through their chemical interactions with the polysulfides. The sulfur electrode with the MoS_2/CNT interlayer possessed an initial capacity of 1237 mA h g^{-1} at 0.5 C and demonstrated a superior cycling stability with a decay of only 0.061% per cycle for 500 cycles at 0.2 C. Furthermore, it also delivered an impressive rate capacity of 784 mA h g^{-1} at 10 C. The fabrication process of the MoS_2/CNT interlayer can be easily scaled up, and the method presents significant potential for the development of high-performance Li–S batteries.

2. Experimental section

2.1. Fabrication of CNT arrays and a MoS_2/CNT functional interlayer

CNT arrays with a tube diameter of 10–20 nm and a height of 300 μm were synthesized on silicon wafers in a chemical vapor deposition system with iron as the catalyst and acetylene as the precursor. The details of the synthesis have been reported in previous publications [30–32]. Continuous CNT films were directly drawn from the CNT arrays by an end-to-end joining mechanism [30,31,33]. MoS_2 powder (50 mg) (Sigma-Aldrich, USA) was dispersed in 200 mL N-methyl-2-pyrrolidinone (NMP) by sonication. After centrifugation, the supernatant containing the MoS_2 nanosheets was diluted with 30 mL alcohol to form the MoS_2 suspension by sonication. The polypropylene film (Celgard 2400) was fixed on a piece of flat glass and then covered with a 2-layer cross-stacked CNT film. The MoS_2 suspension was deposited uniformly onto the CNT film and a thin MoS_2/CNT layer was obtained after the evaporation of the alcohol. This procedure was repeated to obtain the sandwich-structured MoS_2/CNT interlayer with a 20-layer CNT film. Finally, the separators covered with the MoS_2/CNT interlayer were punched into circular shapes with a diameter of 19 mm. Separators covered with a 20-layer CNT film were also prepared as a control sample.

2.2. Preparation of the S cathode

Sulfur powder (Beijing Dk Nano Technology Co., Ltd), carbon black powder (50 nm in diameter, Timcal Ltd., Switzerland), N-methyl-2-pyrrolidinone (NMP), and polyvinylidene difluoride (PVDF) were used as the active material, conducting agent, dispersant, and binder, respectively. The sulfur slurry was prepared by thoroughly mixing sulfur powder, Super P, and PVDF at a weight ratio of 5:4:1 in an NMP solution. They were ground in a mortar for approximately 30 min. The resulting slurry was uniformly spread on an aluminum foil (20 μm in thickness). After drying at 50 °C for approximately 30 min, the electrode sheets were punched into circular discs with a diameter of 10 mm. Before assembly of the cells, all the electrodes were dried again in a vacuum oven overnight at 35 °C. The loading weight of sulfur was about 1.4 mg cm^{-2}, counting for 50 wt% of the electrode.

2.3. Material analysis

The microstructure and morphology of the MoS_2/CNT interlayer were examined by a scanning electron microscope (Sirion 200, FEI) and a transmission electron microscope (Tecnai G2F20, FEI). X-ray photoelectron spectroscopy (XPS) analysis was carried out on a PHI Quantera II surface analysis equipment. The XPS spectra were deconvoluted into Gaussian-Lorentzian-type peaks after applying a Shirley background. The binding energy values were all calibrated using the C 1s peak at 284.8 eV [8,34,35].

2.4. Electrochemical measurement

All electrochemical characterizations were performed using CR2016 coin-type cells. The cell assembly was carried out in an Ar-filled glove box (M. Braun Inert Gas Systems Co. Ltd.) with both moisture and oxygen levels below 0.1 ppm. The S cathodes were the working electrodes, and the lithium foils were used as the counter electrodes for all measurements. The MoS_2/CNT interlayer and CNT interlayer covered with polypropylene film (Celgard 2400) were used as separators, in which the side covered by the MoS_2/CNT or CNT interlayer was towards the S cathode. 1 M LiTFSI solution in dioxolane (DOL) and dimethoxyethane (DME) mixed at a volume ratio of 1:1 with the addition of 0.2 M $LiNO_3$ was used as the electrolyte. The ratio of electrolyte and sulfur was 25 μL mg^{-1} in the cells with the MoS_2/CNT modified separator, CNT modified separator, and the pristine separator. The visual

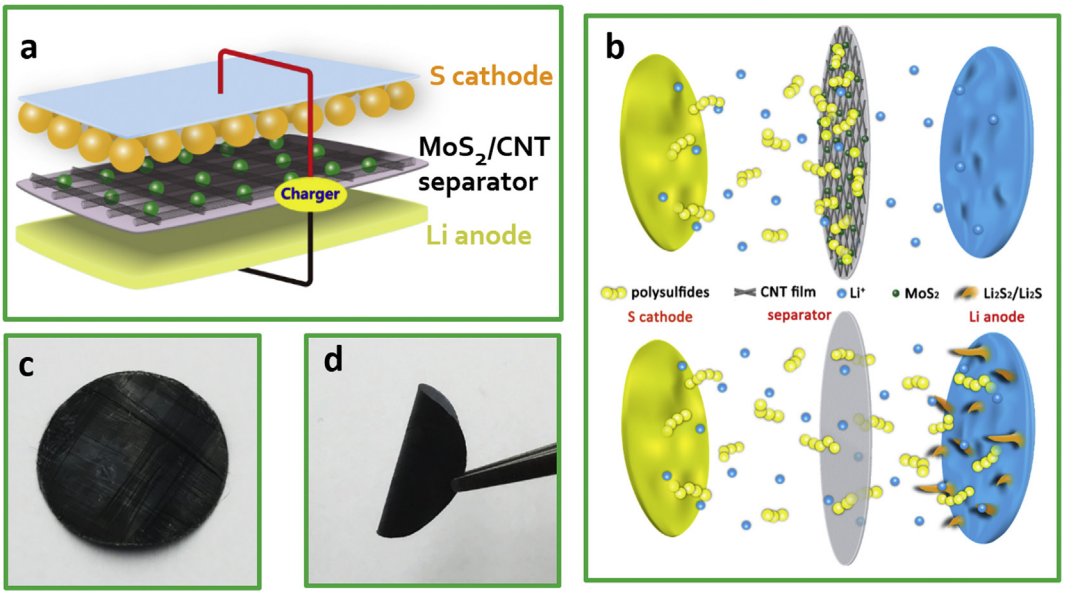

Fig. 1. (a) Schematic diagram of a Li-S cell with the MoS_2/CNT interlayer. (b) Schematic configuration of a Li − S cell with the MoS_2/CNT-interlayer-coated separator (top) and the pristine separator (bottom). (c, d) Photographs of a MoS_2/CNT-interlayer-coated separator showing its high flexibility.

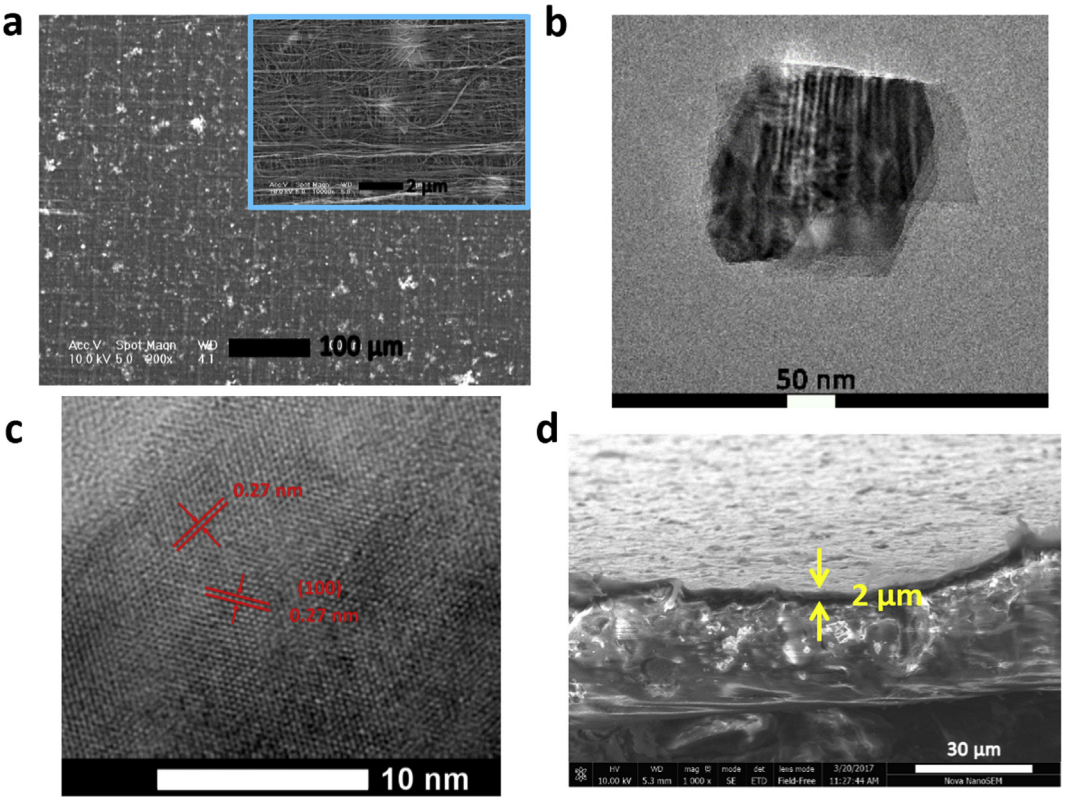

Fig. 2. (a) SEM images of the top surface of a MoS_2/CNT interlayer at low and high magnification (inset). (b) TEM and (c) HRTEM image of MoS_2 nanosheets. (d) Cross-sectional SEM image of a MoS_2/CNT interlayer.

examination of the polysulfide-trapping effect of the MoS_2/CNT interlayer was carried out in a H-type glass cell, in which the right chamber was filled with 0.05 M Li_2S_6 in DOL/DME (v/v = 1:1) solution, and the left chamber was filled with pure DOL/DME. The electrochemical impedance spectroscopy (EIS) measurements were performed using a potentiostat/galvanostat instrument (Princeton PARStat 2273). The charge/discharge measurements were carried on the Land battery test system (Wuhan Land Electronic Co., China) within the voltage window of 1.8–2.6 V at different charge/discharge rates. All the electrochemical tests were performed at room temperature and under an ambient atmosphere.

3. Results and discussion

As illustrated in Fig. 1a, the ultrathin and lightweight MoS_2/CNT interlayer was coated on a separator facing the sulfur electrode in a Li–S battery. For the conventional Li–S cells, the polypropylene/polyethylene separator contained a porous matrix with a pore size of

200–500 nm, which allowed easy infiltration of the electrolyte. However, the polysulfides generated during the charge/discharge processes were highly soluble in the electrolyte. The porous structure could not effectively prevent the polysulfides from shuttling to the anode, which led to corrosion of the Li anode, as shown in the bottom panel of Fig. 1b. To solve this problem, a MoS_2/CNT interlayer was designed to restrain the shuttling of the polysulfides (top panel in Fig. 1b). The commercial MoS_2 powders were first dispersed into NMP under intensive ultrasonication, and then the MoS_2 suspension was deposited uniformly onto the CNT film. By repeating this procedure, a sandwich-structured MoS_2/CNT interlayer with a 20-layer CNT film was obtained. The MoS_2/CNT interlayer demonstrated excellent adhesion to the separator and the interlayer-coated separator had a flat and shiny surface (Fig. 1c). The diameter and areal density of the MoS_2/CNT interlayer (containing 20-layer CNT film) were 19 mm and 0.25 mg cm^{-2}, with 84 wt% of MoS_2. The weight ratio of S/MoS_2 was 1.84, calculated from the diameters and areal densities of the sulfur cathode (10 mm, 1.4 mg cm^{-2}) and the MoS_2/CNT interlayer. The cross-stacked CNT films were highly flexible and possessed a high tensile strength of 180 MPa [36]. Because of the uniform distribution of the MoS_2 nanosheets and the excellent mechanical properties of the CNT film, the MoS_2/CNT-interlayer-coated separator delivered high flexibility, as shown in Fig. 1d. The goal of introducing the MoS_2/CNT interlayer was to alleviate the shuttle effect by both physical and chemical adsorption of the polysulfides.

Top-surface SEM images of the MoS_2/CNT interlayer are shown in Fig. 2a, which revealed uniform dispersion of the MoS_2 nanosheets on the CNT film. The interlayer was also characterized by energy dispersive X-ray (EDX) spectroscopy. The elemental mapping results showed that Mo, S, and C were uniformly distributed, which further confirmed the homogeneous dispersion of MoS_2 in the interlayer (Fig. S1). Fig. 2b and c shows the TEM and high-resolution TEM (HRTEM) images of MoS_2 nanosheets, which illustrate their typical lamellar morphology and highly crystalline structure. A lattice fringe of 0.27 nm was indexed to the (100) plane of MoS_2. The cross-sectional SEM image in Fig. 2d shows that the MoS_2/CNT interlayer was ultrathin and had a thickness of only 2 μm. In the MoS_2/CNT interlayer structure, the cross-stacked CNT film played important roles as a flexible scaffold for anchoring the MoS_2 nanosheets and providing abundant electrical conductive pathways. The MoS_2 nanosheets uniformly dispersed in the CNT film were expected to form chemical bonding with polysulfides and thus alleviate the shuttle effect. With the dual functions of both the CNT film and the MoS_2 nanosheets, electrodes with the MoS_2/CNT interlayer demonstrated improved electrochemical performances.

The cycling performances of the sulfur electrodes with the MoS_2/CNT-interlayer-coated separator, CNT-film-coated separator, and pristine separator at 0.2 C (1 C = 1672 mA g^{-1}) are compared in Fig. 3a. The preparation details of the sulfur electrode can be found in a previous paper [37]. The areal density of the sulfur was 1.4 mg cm^{-2} and the sulfur content in the electrode was 50 wt%. The electrode with the pristine separator showed an initial specific capacity of 1057 mA h g^{-1}, with fast capacity decay to only 327 mA h g^{-1} after 200 cycles. The capacity retention was only 31.0%, indicating a severe shuttle effect and irreversible loss of the active materials. In addition, the deposition of the insulating Li_2S/Li_2S_2 aggregates could also reduce the redox kinetics owing to the lack of conducting pathways. With the introduction of the CNT film, the cycling performance was improved. The electrode exhibited a reversible capacity of 581 mA h g^{-1} after 200 cycles. The improved cycling stability was attributed to the homogenous conductive network provided by the CNT film and, accordingly, the efficient electron transfer and fast redox kinetics. Moreover, the shuttling of the polysulfides was physically restrained by the CNT film to a certain extent. The electrode with the MoS_2/CNT-interlayer-coated separator delivered the best electrochemical performance, with an impressive initial capacity of 1205 mA h g^{-1} and a capacity of 770 mA h g^{-1} after 200 cycles. With the introduction of the MoS_2 nanosheets, more efficient polysulfide trapping was achieved, which might be owing to the strong chemical interactions between the MoS_2 nanosheets and the polysulfides. Combining the advantages of both the CNT film and the MoS_2 nanosheets, the cycling performance of the sulfur electrode with the MoS_2/CNT interlayer was significantly improved. It should be noted that even with the MoS_2/CNT modified separator, sharp capacity decay occurred in the initial cycles, which might be related to self-discharge and shuttle reactions. During the rest period and initial cycles, polysulfides dissolved in the electrolyte and mitigated toward the anode, resulting in a decrease in specific capacity. Approaches to alleviating the fast capacity decay in the initial cycles will be investigated in the future.

The specific capacities of the electrodes with the MoS_2/CNT-interlayer-coated separator and the pristine separator were also investigated at various discharge rates while being charged at a constant rate of 0.2 C. Electrodes with the MoS_2/CNT-interlayer-coated separator demonstrated excellent rate performance (Fig. 3b). They possessed high reversible capacities of 1449, 1066, 986, 923, 902, and 784 mA h g^{-1} at 0.2 C, 0.5 C, 1 C, 2 C, 5 C, and 10 C, respectively. In comparison, electrodes with the pristine separator displayed inferior capacities of 981 and 304 mA h g^{-1} at 0.2 C and 0.5 C, respectively, and completely failed as the rate increased to 1 C. Moreover, when the discharge rate was decreased to 0.2 C, the reversible capability of the electrodes with the MoS_2/CNT interlayer and the pristine separator recovered to 961 and 489 mA h g^{-1}, respectively. The extraordinary rate performance of the electrodes with the MoS_2/CNT-interlayer-coated separator arose because of two factors. First, with the help of highly conductive CNT network, fast charge-transfer kinetics was achieved and the conversion between the insulating discharge products Li_2S/Li_2S_2 and the sulfur materials was accessible. Second, both the CNT film and the MoS_2 nanosheets played important roles in restricting the polysulfide dissolution in the sulfur electrode through physical and/or chemical interaction, so that high reversible capacities were maintained even at high rates.

The galvanostatic charge/discharge curves of the electrodes with the MoS_2/CNT-interlayer-coated separator and the pristine separator in the 1st, 10th, 50th, 100th, 150th, and 200th cycles are shown in Fig. 3c and d. Two typical discharge plateaus were observed, corresponding to the redox reaction from elemental S_8 to polysulfides (Li_2S_n, n = 4–8) at 2.3 V and short-chain Li_2S_2/Li_2S at 2.1 V. Electrodes with the MoS_2/CNT interlayer showed overlapping upper discharge plateaus from the 1st cycle to the 200th cycle, demonstrating excellent polysulfide retention and electrochemical stability (Fig. 3c). Moreover, the lower plateau was very flat, indicating a uniform deposition of Li_2S_2/Li_2S with little kinetic barriers despite their insolubility and low Li^+ diffusivity. The voltage hysteresis between the charge and discharge plateaus was approximately 0.16 V. In contrast, electrodes with the pristine separator displayed shorter upper discharge plateaus as the cycle numbers increased (Fig. 3d), and the capacity retention at the 50th cycle was only 38% of its original value. This demonstrated a relatively large voltage hysteresis of 0.32 V and a severe degree of polarization. In general, the voltage hysteresis is related to the redox reaction kinetics and the reversibility of the system. The low voltage hysteresis in the electrode with the MoS_2/CNT interlayer suggested the fast redox reaction kinetics and high reversibility of the electrode, which were primarily attributed to the following aspects. The CNT film provided a well-connected conductive network for the insulating Li_2S_2/Li_2S and built a physical barrier for the soluble polysulfides. More importantly, the interaction between MoS_2 and the polysulfides further contributed to the high polysulfide retention and stable reversibility of the electrode.

The MoS_2/CNT interlayer also made a great contribution to the prolonged cycling stability of the S cathode. The electrode was charged and discharged at 0.5 C for 500 cycles. The initial specific capacity was 1237 mA h g^{-1}, and a capacity of 648 mA h g^{-1} was obtained at the 500th cycle, with an average capacity decay of 0.061% per cycle (Fig. 3e). Moreover, the extraordinary Coulombic efficiency of 97.3% at

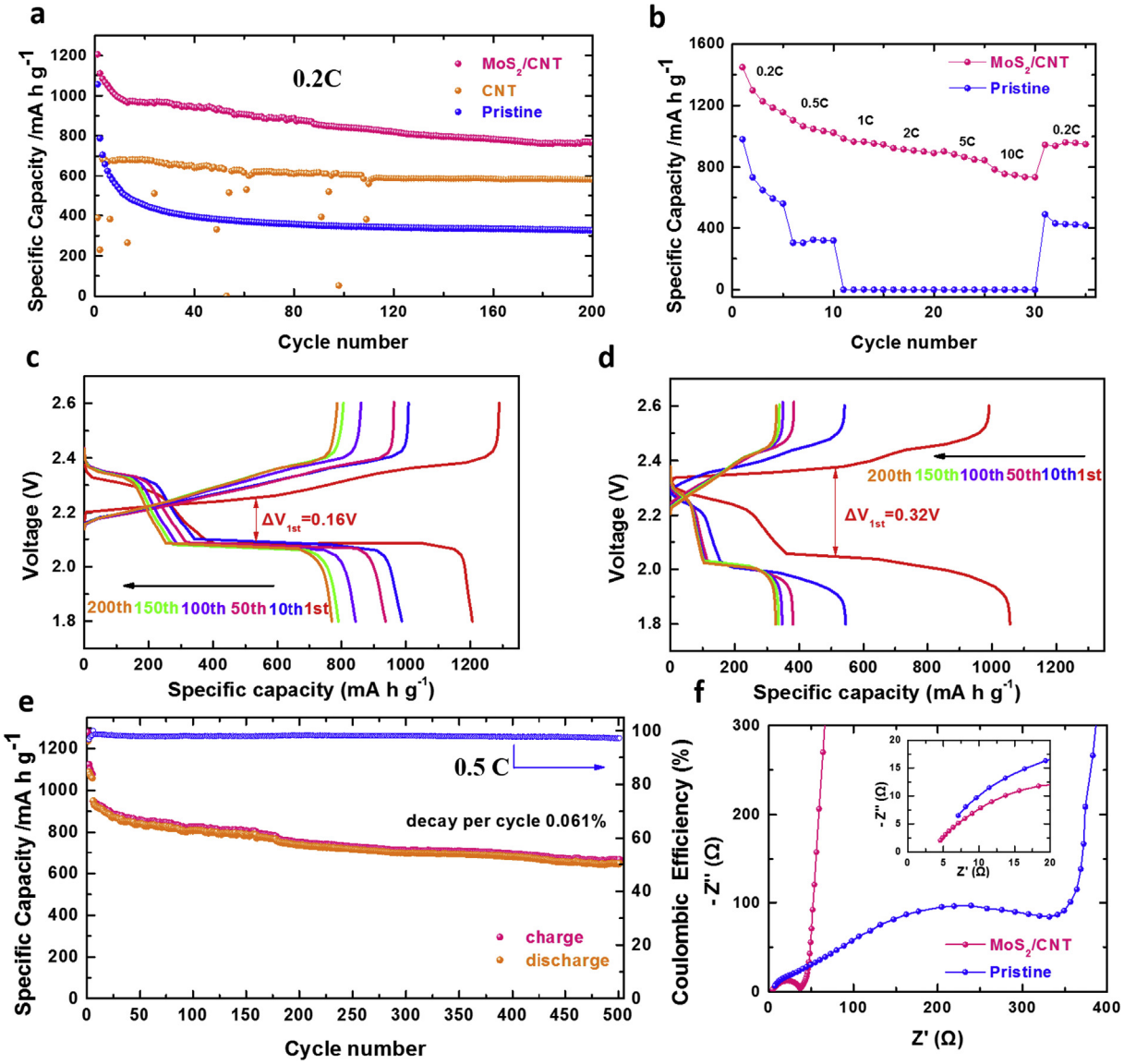

Fig. 3. (a) Cycling performances of the electrodes with a MoS_2/CNT-interlayer-coated separator, CNT film coated separator, and pristine separator at 0.2 C. (b) Rate performances of the electrodes with a MoS_2/CNT-interlayer-coated separator and a pristine separator. Charge/discharge curves of the electrodes with (c) the MoS_2/CNT-interlayer-coated separator and (d) the pristine separator at 0.2 C. (e) Extended cycling performance of the electrode with the MoS_2/CNT-interlayer-coated separator at 0.5 C. (f) EIS spectra of the fresh cells with the MoS_2/CNT-interlayer-coated separator and pristine separator. The inset of (f) is an enlarged view of the high frequency region.

the 500th cycle demonstrated the efficient polysulfide blocking capability of the MoS_2/CNT interlayer [38,39]. As reported in the literature, sulfur electrodes often have a low Coulombic efficiency of less than 90% owing to the serious shuttle effect of polysulfides [40,41]. In this work, with the introduction of the MoS_2/CNT interlayer, the sulfur electrodes exhibited extraordinary long-term cycling performances and high Coulombic efficiency.

The effect of the MoS_2/CNT interlayer on the electrochemical performances of the sulfur electrodes was also studied by EIS. The EIS spectra of the sulfur electrodes with the MoS_2/CNT interlayer and the pristine separator shared a common feature: there was a depressed semicircle in the high to medium frequency region and an inclined line in the low-frequency region (Fig. 3f). The intersections with the real axis in the high-frequency region were related to the electrolyte resistance R_e and the diameters of the semicircles represented the charge transfer resistance R_{ct}. The inset of Fig. 3f shows the enlarged view of the high-frequency range. The R_e values of the sulfur electrodes with the MoS_2/CNT interlayer and the pristine separators were 4.6 Ω and 7.1 Ω, respectively. The larger R_e of the electrode with the pristine separator was owing to the increasing viscosity of the electrolyte that derived from the soluble polysulfides [42], further proving the effective polysulfide trapping capability of the MoS_2/CNT interlayer. The electrode with the MoS_2/CNT interlayer demonstrated a R_{ct} of 36.6 Ω, compared with 331.7 Ω for the electrode with a pristine separator. The reduced charge-transfer resistance in the electrode with the MoS_2/CNT interlayer suggested that the highly conductive CNT film together with the MoS_2 nanosheets could effectively enhance the redox kinetics of polysulfides, facilitate sufficient conversion accessibility of discharge products, and thus promote faster charge transfer [43].

H-type glass cells were employed to visually evaluate the ability of the MoS_2/CNT interlayer to prevent the diffusion of polysulfides. As shown in Fig. 4, the left and right sides of the cell were filled with pure DOL/DME and 0.05 M Li_2S_6 in DOL/DME, respectively. Driven by the concentration gradient, Li_2S_6 tended to diffuse through the separator from the right side to the left side. In Fig. 4a–c, two glass cells were separated by the MoS_2/CNT-interlayer-coated separator. There was no

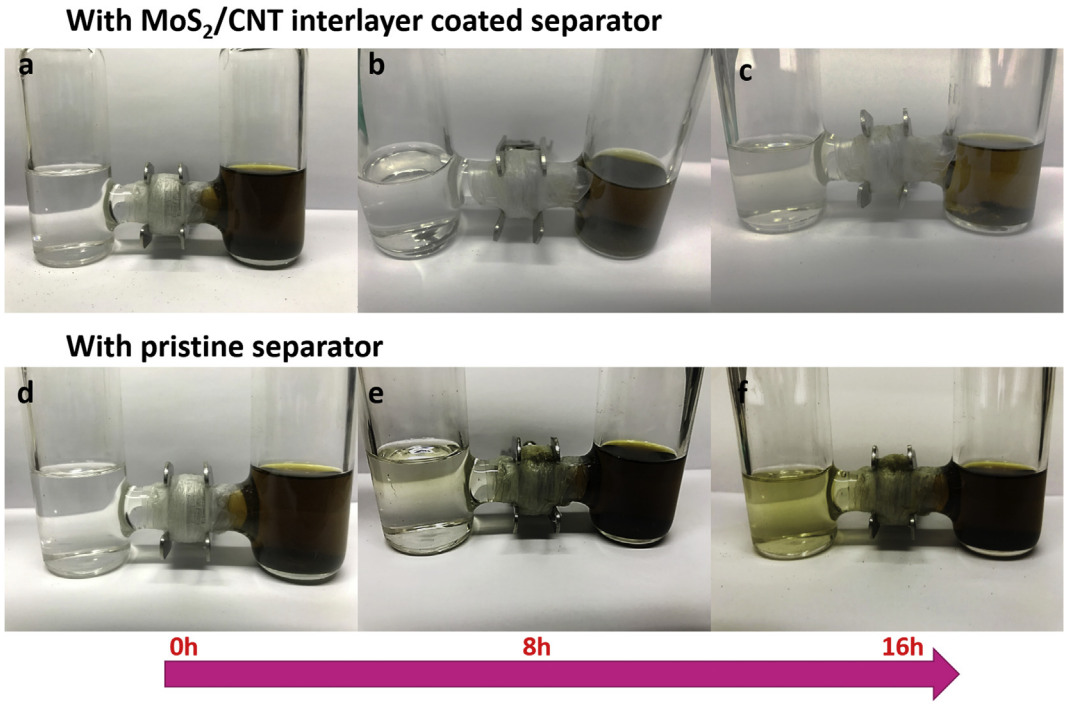

Fig. 4. Photographs of the H-type glass cells with pure DOL/DME (left chamber) and polysulfides (Li_2S_6) in DOL/DME (right chamber), separated by the MoS_2/CNT interlayer (a–c) and the pristine separator (d–f).

obvious color change in the left cell even after 16 h, indicating that polysulfide diffusion was effectively restrained by the MoS_2/CNT interlayer. For comparison, two cells were separated by the pristine separator (Fig. 4d–f). The left cell became light yellow after 8 h (Fig. 4e) and then dark yellow after 16 h (Fig. 4f). These results indicated that the polysulfides were able to diffuse easily across the pristine separator in a Li–S system and reach the lithium metal, leading to severe loss of the active materials and corrosion of the lithium metal.

XPS analysis of the MoS_2/CNT interlayer before and after cycling at 0.2 C was performed to investigate any chemical interaction between the MoS_2 nanosheets and the polysulfides. In the Mo 3d spectrum of the MoS_2/CNT interlayer before cycling, the doublets at 229.8 eV and 232.9 eV were assigned to Mo $3d_{2/5}$ and Mo $3d_{2/3}$ of Mo^{4+}, respectively (Fig. 5a). The peak located at 226.6 eV corresponded to the S 2s of the divalent sulfide ions (S^{2-}) [28]. For the MoS_2/CNT interlayer after cycling, the binding energies of Mo $3d_{2/5}$ and Mo $3d_{2/3}$ of Mo^{4+} slightly shifted to lower values of 229.2 eV and 232.3 eV, suggesting the Mo–S_n^{2-} chemical interaction [44,45]. The XPS results directly proved the chemical interaction between the MoS_2 nanosheets and the polysulfides, which effectively entrapped the polysulfides during cycling and contributed to the enhanced electrochemical performances of the sulfur electrodes.

The nanoscale interfacial interactions between MoS_2 and lithium polysulfides were further validated from a computational perspective. First-principles calculations were performed using the projector augmented wave method as implemented in the Vienna ab initio simulation package (VASP) [46,47]. The Perdew–Burke–Ernzerhof functional was used to treat the electron exchange and correlations [48]. The convergence criterion for the total energy and the Hellmann-Feynman force were 10^{-5} eV and 0.01 eV/Å, respectively. More calculation details are specified in the supporting information. The binding geometries and energies of a Li_2S_4 molecule on CNT and MoS_2 were obtained. CNT,

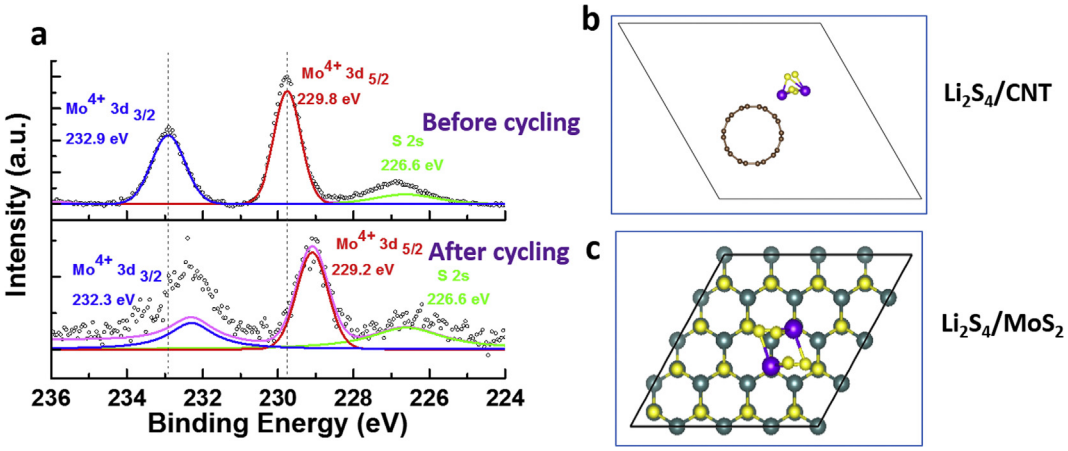

Fig. 5. (a) XPS spectra of the MoS_2/CNT interlayer before and after cycling. Binding geometries (top view) and energies of a Li_2S_4 molecule on (b) CNT and (c) MoS_2. Brown, yellow, purple, and green balls represent C, S, Li, and Mo atoms, respectively. (For interpretation of the references to color in this figure legend, the reader is referred to the Web version of this article.)

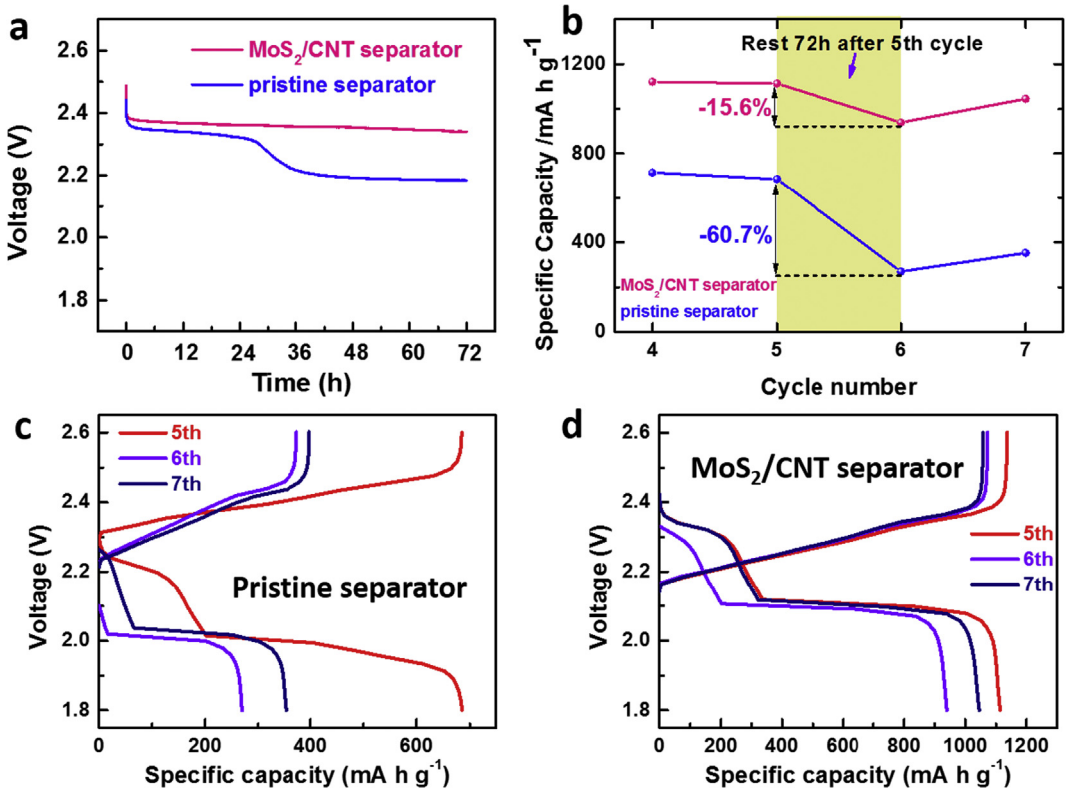

Fig. 6. Self-discharge behavior of the electrodes with the MoS_2/CNT-interlayer-coated separator and the pristine separator. The cells were rested for 72 h after the 5th cycle. (a) Open-circuit voltage profiles during the rest time. (b) Cycling performance of the electrodes. Charge/discharge voltage profiles of the electrodes with (c) the pristine separator and (d) the MoS_2/CNT-interlayer-coated separator at 0.2 C before (5th cycle) and after (6th and 7th cycles) rest.

mainly formed by nonpolar C – C bond, only provided a limited binding energy of 0.46 eV (Fig. 5b). In contrast, a higher binding energy of 1.50 eV (top view in Fig. 5c and side view in Fig. S2) was generated between MoS_2 and Li_2S_4, implying the strong chemical interaction between the MoS_2 nanosheets and the polysulfides [3,45,49].

Self-discharge resulting from the shuttle effect is one of the major drawbacks in Li-S batteries. In general, about 30% of the capacity self-discharges within several hours, which hinders the practical utilization in various devices [50,51]. The problem of self-discharge can be alleviated by the MoS_2/CNT interlayer. Electrodes with the MoS_2/CNT-interlayer-coated separator and the pristine separator were rested for 72 h after the 5th cycle at 0.2 C, followed by the subsequent discharge/charge at 0.2C. Fig. 6a depicts their open-circuit voltage profiles. For the cell with the pristine separator, there was obvious voltage decay from 2.38 to 2.18 V during the 72 h rest, implying the severe spontaneous reduction from the high-order polysulfides to the low-order polysulfides [51]. In contrast, the self-discharge was sufficiently inhibited by the MoS_2/CNT interlayer, and the voltage only experienced a small decrease from 2.38 to 2.34 V during the 72 h rest. The corresponding cycling performances after the 72 h rest are shown in Fig. 6b. After rest (at the 6th cycle), the capacity of the electrode with the pristine separator sharply dropped by 60.7% of the original capacity, whereas for the electrode with the MoS_2/CNT-interlayer-coated separator, the decline rate was only 15.6%. Even though there was an increasing tendency in the discharge capacities at the 7th cycle for both cells after rest, the reversibility of the high voltage plateau was poor and the retention of the specific capacity was low (54% of the capacity before rest) for the cell with the pristine separator (Fig. 6c) because of the inferior redox kinetics owing to the dissolution of polysulfides and the deposition of the insulating Li_2S/Li_2S_2 [40]. In contrast, the high voltage plateau for the 7th cycle (after rest) nearly overlapped with that of the 5th cycle (before rest) for the cell with the MoS_2/CNT interlayer (Fig. 6d). The capacity retention reached 94%, which resulted from the suppression of the self-discharge, effective trapping of the polysulfides, and excellent conductivity of the CNT film. Moreover, the high voltage plateau after rest became slightly smaller for the electrode with the MoS_2/CNT interlayer (Fig. 6d), whereas it almost vanished for the electrode with the pristine separator (Fig. 6c) owing to the conversion from the high-order polysulfides to low-order polysulfides during the self-discharge process. The significant suppression of the self-discharge resulted from the excellent conductivity, physical barrier, and chemical interaction of the MoS_2/CNT interlayer.

The morphologies of the cycled lithium anodes were further studied by SEM to investigate the ability of the MoS_2/CNT interlayer to suppress the dissolution of polysulfides. As shown in Fig. 7a and b, the cycled Li anode in the cell with the MoS_2/CNT interlayer had a relatively smooth surface. In contrast, the cycled Li anode in the cell with the pristine separator had a rough surface with fiber-like reaction products (Fig. 7d–e). The insets in Fig. 7b and e display the EDX results of the lithium foils. The intensity of the sulfur peak for the cell with MoS_2/CNT interlayer was much smaller than that with the pristine separator, suggesting that the deposition of Li_2S and Li_2S_2 on the Li anode was greatly reduced in the cell with the MoS_2/CNT interlayer. The cross-sectional SEM images of the cycled Li anodes in the cells with the MoS_2/CNT interlayer and the pristine separator in Fig. 7c and f show the passivation layers with a thicknesses of 25 and 81 μm, respectively. The passivation layer on the Li anode surface was formed owing to the fast dissolution/deposition of polysulfides and Li_2S/Li_2S_2 and the reaction between the lithium polysulfides and electrolyte additive [2,52,53]. With the introduction of the MoS_2/CNT interlayer, the repeated cracking and reforming of the passivation layer on the Li anode was significantly restrained and the pulverization of the Li anode was significantly depressed, leading to a thinner passivation layer [54]. The SEM images of the cycled Li anodes indicated that the MoS_2/CNT interlayer could effectively suppress the shuttle effect and side reactions, and thus, dramatically improved the electrochemical

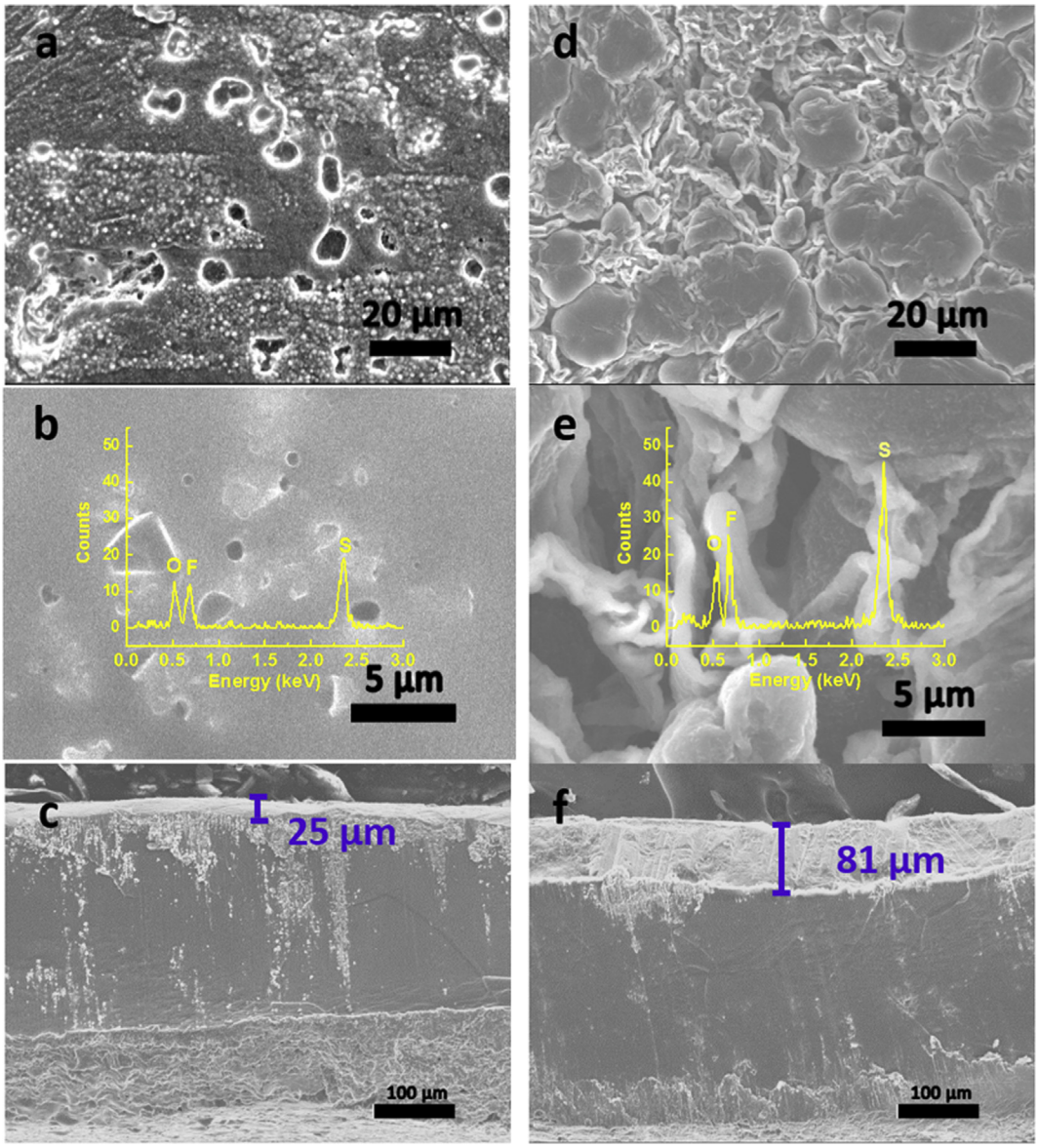

Fig. 7. SEM images of the cycled Li anodes with (a–c) the MoS_2/CNT-interlayer-coated separator and (d–f) the pristine separator. (a, b, d, e) are the top surface images and (c, f) are the cross-sectional images. Insets of (b, e) are the corresponding EDX spectra.

Table 1
Comparison of the electrochemical performances of sulfur electrodes with various interlayers or modified separators reported in the literature.

Samples	Areal density/mg cm^{-2}	S content/wt%	Capacity at high rate/mA h g^{-1}	Capacity at low rate/mA h g^{-1}	Reference
MoS_2/CNT interlayer	0.25	50% 1.4 mg cm^{-2}	784 (10C)	1237 (0.5C) −0.061% (500th) decay per cycle	This work
Nafion	0.7	50% 0.53 mg cm^{-2}	533 (5C)	781 (1C) −0.08% (500th) decay per cycle	[55]
B-rGO coated separator	0.2–0.3	56% 1.45–1.56 mg cm^{-2}	< 600 (3C)	1228 (0.1C) −0.1532% (300th) decay per cycle	[56]
CNF-T as interlayer	0.5–0.6	60% 0.8 mg cm^{-2}	630 (2C)	1328 (0.2C) −0.121% (500th) decay per cycle	[57]
PEDOT:PSS coated separator	0.07	64% 0.9–1.1 mg cm^{-2}	690 (2C)	985 (0.25C) −0.0364% (1000th) decay per cycle	[58]
CNTs network interlayer	1.69	70% 0.974 mg cm^{-2}	466 (2.5C)	1658 (0.25C) −0.665% (100th)	[59]
N/P dual doped graphene coated separator	ca. 1.0 ± 0.1	70%	634 (2C)	1158.3 (1C) - 0.0898% (500th)	[60]

performances of the electrodes.

A comparison of the electrochemical performance of the sulfur electrode with the MoS_2/CNT interlayer and other sulfur electrodes with different interlayers or separators reported in the literature is shown in Table 1 [55–60]. The electrode with the MoS_2/CNT interlayer possessed the best rate performances (784 mA h g^{-1}) at a high rate of 10 C and also delivered better long-term cycle stability (1237 mA h g^{-1} at 0.5 C with a capacity decay of 0.061% per cycle for 500 cycles) than those reported in the literature. The excellent electrochemical properties of electrode with the MoS_2/CNT interlayer can be attributed to the following aspects. First, the cross-stacked CNT film provided a homogeneous and conductive network for the efficient electron transfer and built a physical barrier against polysulfide dissolution. Moreover, the MoS_2 nanosheets formed effective chemical bonding with the polysulfides, thus reducing the shuttle effect and improving the electrochemical performances of the electrode.

4. Conclusion

We demonstrated a simple and feasible approach to improve the electrochemical performances of Li-S batteries. An interlayer consisting of MoS_2 nanosheets and cross-stacked CNT film was introduced between the sulfur cathode and the pristine separator. The ultrathin and lightweight MoS_2/CNT interlayer not only provided the integrated conductive pathways for electrons, but also built a physical barrier to prevent the diffusion of polysulfides. More importantly, it also facilitated the chemical interaction and binding between the polysulfides and the MoS_2 nanosheets. The electrode with the MoS_2/CNT interlayer exhibited a high initial capacity of 1205 mA h g^{-1} at 0.2 C and an impressive rate capability of 784 mA h g^{-1} at 10 C. Remarkably, the superior cycling stability was delivered at 0.5 C, with a capacity decay as low as 0.061% per cycle for 500 cycles. Moreover, the self-discharge problems associated with sulfur electrodes was dramatically suppressed by the MoS_2/CNT interlayer. The introduction of the MoS_2/CNT interlayer greatly improved the utilization of the active materials and efficiently suppressed the shuttle effect of the polysulfides. Furthermore, the fabrication procedure of the MoS_2/CNT interlayer was easy to implement and feasible. Therefore, the use of a MoS_2/CNT interlayer in sulfur electrodes has a great potential to enhance the electrochemical performances of Li-S batteries.

Acknowledgments

This work was supported by the NSFC (Grant No. 51472141 and 51788104), the National Basic Research Program of China (Grant No. 2016YFA0301001 and 2017YFA0205800), the Beijing Municipal Science and Technology Commission (Grant No. D161100002416003), and Tsinghua University Tutor Research Fund.

Appendix A. Supplementary data

Supplementary data related to this article can be found at http://dx.doi.org/10.1016/j.jpowsour.2018.04.015.

References

[1] F. Wang, X. Wu, C. Li, Y. Zhu, L. Fu, Y. Wu, X. Liu, Energy Environ. Sci. 9 (2016) 3570–3611.
[2] R. Cao, W. Xu, D. Lv, J. Xiao, J. Zhang, Adv. Energy Mater. 5 (2015) 1402273.
[3] E.P. Kamphaus, P.B. Balbuena, J. Phys. Chem. C 120 (2016) 4296–4305.
[4] Y. Xiang, J. Li, J. Lei, D. Liu, Z. Xie, D. Qu, K. Li, T. Deng, H. Tang, ChemSusChem 9 (2016) 3023–3039.
[5] A. Rosenman, E. Markevich, G. Salitra, D. Aurbach, A. Garsuch, F.F. Chesneau, Adv. Energy Mater. (2015) 1500212.
[6] A. Manthiram, Y. Fu, S. Chung, C. Zu, Y. Su, Chem. Rev. 114 (2014) 11751–11787.
[7] W. Kong, L. Yan, Y. Luo, D. Wang, K. Jiang, Q. Li, S. Fan, J. Wang, Adv. Funct. Mater. (2017) 1606663.
[8] L. Sun, D. Wang, Y. Luo, W. Kong, Y. Wu, L. Zhang, K. Jiang, Q. Li, Y. Zhang, J. Wang, S. Fan, ACS Nano 10 (2016) 1300–1308.
[9] W. Kong, L. Sun, Y. Wu, K. Jiang, Q. Li, J. Wang, S. Fan, Carbon 96 (2016) 1053–1059.
[10] Z. Li, J. Zhang, X.W.D. Lou, Angew. Chem. Int. Ed. 54 (2015) 12886–12890.
[11] G. He, B. Mandlmeier, J. Schuster, L.F. Nazar, T. Bein, Chem. Mater. 26 (2014) 3879–3886.
[12] G. Zhou, E. Paek, G.S. Hwang, A. Manthiram, Nat. Commun. 6 (2015) 7760.
[13] C. Yang, Y. Yin, H. Ye, K. Jiang, J. Zhang, Y. Guo, Acs Appl. Mater. Inter. 6 (2014) 8789–8795.
[14] J. Schuster, G. He, B. Mandlmeier, T. Yim, K.T. Lee, T. Bein, L.F. Nazar, Angew. Chem. Int. Ed. 51 (2012) 3591–3595.
[15] H. Li, M. Sun, T. Zhang, Y. Fang, G. Wang, J. Mater. Chem. 2 (2014) 18345–18352.
[16] W. Zhou, Y. Yu, H. Chen, F.J. DiSalvo, H.D. Abruna, J. Am. Chem. Soc. 135 (2013) 16736–16743.
[17] Y. Fu, A. Manthiram, J. Phys. Chem. C 116 (2012) 8910–8915.
[18] Z. Chang, H. Dou, B. Ding, J. Wang, Y. Wang, X. Hao, D.R. MacFarlane, J. Mater. Chem. 5 (2017) 250–257.
[19] Z.W. Seh, W. Li, J.J. Cha, G. Zheng, Y. Yang, M.T. McDowell, P. Hsu, Y. Cui, Nat. Commun. 4 (2013) 1311.
[20] Y. Su, A. Manthiram, Nat. Commun. 3 (2012) 1166.
[21] T. Jeong, Y.H. Moon, H. Chun, H.S. Kim, B.W. Cho, Y. Kim, Chem. Commun. 49 (2013) 11107–11109.
[22] X. Liang, C. Hart, Q. Pang, A. Garsuch, T. Weiss, L.F. Nazar, Nat. Commun. 6 (2015) 5682.
[23] Z. Xiao, Z. Yang, L. Wang, H. Nie, M. Zhong, Q. Lai, X. Xu, L. Zhang, S. Huang, Adv. Mater. 27 (2015) 2891–2898.
[24] L. Kong, H. Peng, J. Huang, W. Zhu, G. Zhang, Z. Zhang, P. Zhai, P. Sun, J. Xie, Q. Zhang, Energy Storage Mater. 8 (2017) 153–160.
[25] T. Zhao, Y. Ye, X. Peng, G. Divitini, H. Kim, C. Lao, P.R. Coxon, K. Xi, Y. Liu, C. Ducati, R. Chen, R.V. Kumar, Adv. Funct. Mater. 26 (2016) 8418–8426.
[26] H. Peng, Z. Zhang, J. Huang, G. Zhang, J. Xie, W. Xu, J. Shi, X. Chen, X. Cheng, Q. Zhang, Adv. Mater. 28 (2016) 9551.
[27] E.P. Kamphaus, P.B. Balbuena, J. Phys. Chem. C 120 (2016) 4296–4305.
[28] Z. Li, S. Deng, R. Xu, L. Wei, X. Su, M. Wu, Electrochim. Acta 252 (2017) 200–207.
[29] P.T. Dirlam, J. Park, A.G. Simmonds, K. Domanik, C.B. Arrington, J.L. Schaefer, V.P. Oleshko, T.S. Kleine, K. Char, R.S. Glass, C.L. Soles, C. Kim, N. Pinna, Y. Sung, J. Pyun, Acs Appl. Mater. Inter. 8 (2016) 13437–13448.
[30] K. Jiang, J. Wang, Q. Li, L. Liu, C. Liu, S. Fan, Adv. Mater. 23 (2011) 1154–1161.
[31] X.B. Zhang, K.L. Jiang, C. Teng, P. Liu, L. Zhang, J. Kong, T.H. Zhang, Q.Q. Li, S.S. Fan, Adv. Mater. 18 (2006) 1505.
[32] K.L. Jiang, Q.Q. Li, S.S. Fan, Nature 419 (2002) 801.
[33] L. Yan, K. Wang, S. Luo, H. Wu, Y. Luo, Y. Yu, K. Jiang, Q. Li, S. Fan, J. Wang, J. Mater. Chem. 5 (2017) 4047–4057.
[34] M. Li, Y. Wu, F. Zhao, Y. Wei, J. Wang, K. Jiang, S. Fan, Carbon 69 (2014) 444–451.
[35] D. Wang, K. Wang, H. Wu, Y. Luo, L. Sun, Y. Zhao, J. Wang, L. Jia, K. Jiang, Q. Li, S. Fan, J. Wang, Carbon 132 (2018) 370–379.
[36] K. Liu, Y. Sun, P. Liu, X. Lin, S. Fan, K. Jiang, Adv. Funct. Mater. 21 (2011) 2721–2728.
[37] L. Sun, W. Kong, M. Li, H. Wu, K. Jiang, Q. Li, Y. Zhang, J. Wang, S. Fan, Nanotechnology 27 (2016) 754017.
[38] Q. Pang, L.F. Nazar, ACS Nano 10 (2016) 4111–4118.
[39] J. Yoo, S. Cho, G.Y. Jung, S.H. Kim, K. Choi, J. Kim, C.K. Lee, S.K. Kwak, S. Lee, Nano Lett. 16 (2016) 3292–3300.
[40] A. Manthiram, Y. Fu, S.H. Chung, C. Zu, Y.S. Su, Chem. Rev. (2014) 11757–11781.
[41] J. Guo, Y. Xu, C. Wang, Nano Lett. 11 (2011) 4288–4294.
[42] Z. Deng, Z. Zhang, Y. Lai, J. Liu, J. Li, Y. Liu, J. Electrochem. Soc. 160 (2013) A553–A558.
[43] Z. Yuan, H. Peng, T. Hou, J. Huang, C. Chen, D. Wang, X. Cheng, F. Wei, Q. Zhang, Nano Lett. 16 (2016) 519–527.
[44] Z.A. Ghazi, X. He, A.M. Khattak, N.A. Khan, B. Liang, A. Iqbal, J. Wang, H. Sin, L. Li, Z. Tang, Adv. Mater. (2017) 1606817.
[45] J. Sun, Y. Sun, M. Pasta, G. Zhou, Y. Li, W. Liu, F. Xiong, Y. Cui, Adv. Mater. 28 (2016) 9797.
[46] P. Kackell, J. Furthmuller, F. Bechstedt, G. Kresse, J. Hafner, Phys. Rev. B 54 (1996) 10304–10307.
[47] G. Kresse, J. Hafner, Phys. Rev. B 47 (1993) 558–561.
[48] J.P. Perdew, K. Burke, M. Ernzerhof, Phys. Rev. Lett. 77 (1996) 3865–3868.
[49] H. Wang, Q. Zhang, H. Yao, Z. Liang, H. Lee, P. Hsu, G. Zheng, Y. Cui, Nano Lett. 14 (2014) 7138–7144.
[50] M.L. Gordin, F. Dai, S. Chen, T. Xu, J. Song, D. Tang, N. Azimi, Z. Zhang, D. Wang, Acs Appl. Mater. Inter. 6 (2014) 8006–8010.
[51] J. Huang, T. Zhuang, Q. Zhang, H. Peng, C. Chen, F. Wei, ACS Nano 9 (2015) 3002–3011.
[52] G. Zhou, Y. Zhao, A. Manthiram, Adv. Energy Mater. 5 (2015) 1402263.
[53] S. Xiong, K. Xie, Y. Diao, X. Hong, J. Power Sources 246 (2014) 840–845.
[54] K. Xie, K. Yuan, K. Zhang, C. Shen, W. Lv, X. Liu, J. Wang, B. Wei, Acs Appl. Mater. Inter. 9 (2017) 4605–4613.
[55] J. Huang, Q. Zhang, H. Peng, X. Liu, W. Qian, F. Wei, Energy Environ. Sci. 7 (2014) 347–353.
[56] F. Wu, J. Qian, R. Chen, Y. Ye, Z. Sun, Y. Xing, L. Li, J. Mater. Chem. 4 (2016) 17033–17041.
[57] G. Liang, J. Wu, X. Qin, M. Liu, Q. Li, Y. He, J. Kim, B. Li, F. Kang, Acs Appl. Mater. Inter. 8 (2016) 23105–23113.
[58] S.A. Abbas, M.A. Ibrahem, L. Hu, C. Lin, J. Fang, K.M. Boopathi, P. Wang, L. Li, C. Chu, J. Mater. Chem. 4 (2016) 9661–9669.
[59] M. Li, W. Wahyudi, P. Kumar, F. Wu, X. Yang, H. Li, L. Li, J. Ming, Acs Appl. Mater. Inter. 9 (2017) 8047–8054.
[60] X. Gu, C. Tong, C. Lai, J. Qiu, X. Huang, W. Yang, B. Wen, L. Liu, Y. Hou, S. Zhang, J. Mater. Chem. 3 (2015) 16670–16678.